Ocean acidification affects coral growth by reducing skeletal density

Nathaniel R. Mollica[a,b,1], Weifu Guo[b,1], Anne L. Cohen[b], Kuo-Fang Huang[c], Gavin L. Foster[d], Hannah K. Donald[d], and Andrew R. Solow[e]

[a]Massachusetts Institute of Technology–Woods Hole Oceanographic Institution Joint Program in Oceanography, Woods Hole, MA 02543; [b]Department of Geology and Geophysics, Woods Hole Oceanographic Institution, Woods Hole, MA 02543; [c]Institute of Earth Sciences, Academia Sinica, Nangang, Taipei 11529, Taiwan; [d]Ocean and Earth Science, University of Southampton, SO14 3ZH Southampton, United Kingdom; and [e]Marine Policy Center, Woods Hole Oceanographic Institution, Woods Hole, MA 02543

Edited by Nancy Knowlton, Smithsonian Institution, Washington, DC, and approved December 11, 2017 (received for review July 18, 2017)

Ocean acidification (OA) is considered an important threat to coral reef ecosystems, because it reduces the availability of carbonate ions that reef-building corals need to produce their skeletons. However, while theory predicts that coral calcification rates decline as carbonate ion concentrations decrease, this prediction is not consistently borne out in laboratory manipulation experiments or in studies of corals inhabiting naturally low-pH reefs today. The skeletal growth of corals consists of two distinct processes: extension (upward growth) and densification (lateral thickening). Here, we show that skeletal density is directly sensitive to changes in seawater carbonate ion concentration and thus, to OA, whereas extension is not. We present a numerical model of *Porites* skeletal growth that links skeletal density with the external seawater environment via its influence on the chemistry of coral calcifying fluid. We validate the model using existing coral skeletal datasets from six *Porites* species collected across five reef sites and use this framework to project the impact of 21st century OA on *Porites* skeletal density across the global tropics. Our model predicts that OA alone will drive up to 20.3 ± 5.4% decline in the skeletal density of reef-building *Porites* corals.

coral calcification | ocean acidification | skeletal density | biomineralization

Coral reefs are among the most diverse ecosystems on Earth, with enormous cultural, ecological, and economic value. The calcium carbonate (aragonite) skeletons of stony corals are the main building blocks of the reef structure and provide food, shelter, and substrate for a myriad of other organisms. However, corals are vulnerable to environmental changes, including ocean acidification, which reduces the concentration of carbonate ions ($[CO_3^{2-}]$) that corals need to build their skeletons (1, 2). Under the "business as usual" emissions scenario, seawater $[CO_3^{2-}]$ is projected to decline across the global tropics by ∼100 μmol/kg by 2100 (1, 3, 4), almost halving preindustrial concentration. Predictions based on abiogenic precipitation experiments imply an associated decrease in the precipitation rate of aragonite of ∼48% (5). Such predictions raise concerns that many coral reefs will shift from a state of net carbonate accretion to net dissolution (3). Nevertheless, both laboratory manipulation experiments rearing corals under high pCO_2 conditions and field studies of naturally low-pH reefs that are designed to explore the impact of ocean acidification on coral calcification, have yielded inconsistent results (e.g., refs. 6–13). Field-based measurements of calcification rates of corals inhabiting naturally low pH reefs today vary widely from sharp decreases in calcification rate with decreasing pH to no significant response. For example, a nonlinear response of *Porites astreoides* to declines in seawater aragonite saturation state (Ω_{sw}) was observed in the Yucatan Ojos, with no change in calcification rate at $\Omega_{sw} > 1$ and a sharp decline in calcification when conditions become undersaturated (9). At CO_2 vent sites on the volcanic island Maug (northern Mariana Islands), a significant decline in *Porites* calcification rate was observed between ambient and mid Ω_{sw} conditions (3.9 and 3.6, respectively), yet no change between the mid and low ($\Omega_{sw} = 3.4$) conditions (14). On other reefs, calcification rates are constant across the Ω_{sw} range. For example, *Porites* calcification at Milne Bay (Papua New Guinea) CO_2 vents showed no significant change between Ω_{sw} of 3.5 and 2.9 (10), and on Palau, no change in calcification rate of two massive genera of coral (*Porites* and *Favia*) was observed across an Ω_{sw} gradient of 3.7–2.4 (11).

These results have raised questions about the potential for adaptation, acclimation, and/or the role of non-pH factors in modulating the influence of ocean acidification in natural systems, confounding efforts to predict reef calcification responses to 21st century ocean acidification (13). The reefs in the studies discussed above are very different both compositionally and environmentally, and in each case, the low Ω_{sw} is a result of different factors (e.g., CO_2 vents vs. freshwater seeps). However, one commonality among these studies is that calcification rates are reported for massive species by measuring linear extension and skeletal density in cores extracted from living colonies. The product of annual linear extension and mean skeletal density is used to estimate the annual calcification rate (15). While this measure provides an accurate estimate of the annual amount of $CaCO_3$ produced by the coral, it does not account for the possibility that density and extension could be influenced by different factors (e.g., seawater chemistry, light exposure, nutrient level). Here, we combine measurements of seawater saturation state, skeletal growth of *Porites*, and constraints on the coral's calcifying fluid composition to examine the impact of ocean acidification on each skeletal growth parameter separately.

Significance

Ocean acidification (OA) threatens coral reef futures by reducing the concentration of carbonate ions that corals need to construct their skeletons. However, quantitative predictions of reef futures under OA are confounded by mixed responses of corals to OA in experiments and field observations. We modeled the skeletal growth of a dominant reef-building coral, *Porites*, as a function of seawater chemistry and validated the model against observational data. We show that OA directly and negatively affects one component of the two-step growth process (density) but not the other (linear extension). Combining our growth model with Global Climate Model output, we show that skeletal density of *Porites* corals could decline by up to 20.3% over the 21st century solely due to OA.

Author contributions: N.R.M., W.G., and A.L.C. designed research; N.R.M., W.G., A.L.C., K.-F.H., G.L.F., H.K.D., and A.R.S. performed research; A.L.C., K.-F.H., and G.L.F. contributed new reagents/analytical tools; N.R.M. and W.G. analyzed data; and N.R.M., W.G., and A.L.C. wrote the paper.

The authors declare no conflict of interest.

This article is a PNAS Direct Submission.

[1]To whom correspondence may be addressed. Email: nmollica@whoi.edu or wfguo@whoi.edu.

This article contains supporting information online at www.pnas.org/lookup/suppl/doi:10.1073/pnas.1712806115/-/DCSupplemental.

Results and Discussion

***Porites* Skeletal Density but Not Extension Is Sensitive to Ocean Acidification.** Extension, density, and calcification rates were quantified in nine *Porites* skeletal cores from four Pacific reefs (Palau, Donghsa Atoll, Green Island, and Saboga) representing average Ω_{sw} ranging from ~2.4 to ~3.9 (Fig. 1). We observed no correlation between annual calcification rates and Ω_{sw} either within or between reef sites. However, coral calcification does not take place directly from ambient seawater but within an extracellular calcifying fluid or medium (ECM) that is located between the coral skeleton and its calicoblastic cell membrane (16–18). The carbonate chemistry of the ECM is strongly regulated by corals and can differ significantly from ambient seawater (19, 20). Most notably, pH of the ECM is elevated above ambient seawater by up to 1 unit (21–25). Geochemical proxy data suggest that dissolved inorganic carbon (DIC) concentrations in *Porites* ECM are also elevated relative to seawater (e.g., by a factor of ~1.4 or ~2.6) (26, 27), although in vivo microelectrode measurements of other coral species imply a DIC concentration in the ECM similar to seawater (28). A combination of elevated pH and DIC leads to higher aragonite saturation state in the ECM (Ω_{ECM}), which exerts direct control on the rate of aragonite precipitation by the coral.

To estimate Ω_{ECM} of our coral cores, we first reconstructed the pH of coral ECM based on their boron isotope compositions and then combined these pH estimates with in situ measurements of seawater temperature, salinity, and DIC concentration. An elevation factor (α) of 2 is adopted to account for the elevation of DIC concentration within the ECM relative to seawater values (*SI Text*). Our estimated Ω_{ECM} for these cores varies from 11.6 ± 0.9 to 17.8 ± 2.0, ~3.5–4.6 times higher than the Ω_{sw} in which the corals grew. Nevertheless, we observe no correlation between coral calcification rates and Ω_{ECM} (Fig. 1*B*). Instead, when we deconvolve calcification into skeletal extension and skeletal density, a significant correlation is observed between coral skeletal density and Ω_{ECM} and also, skeletal density and Ω_{sw} (Fig. 1 *C* and *D*). Skeletal extension, however, does not show a statistically significant correlation with Ω_{ECM} or Ω_{sw} (Fig. 1 *E* and *F*). Correlations between skeletal density and Ω_{sw}, similar to that observed in our data, have also been reported in other field studies (9–11, 29), including at some of the key ocean acidification study sites (e.g., CO_2 vents in Italy, Papua New Guinea, and the Caribbean Ojos) (9, 10, 29), but not all (14, 30) (Fig. S1).

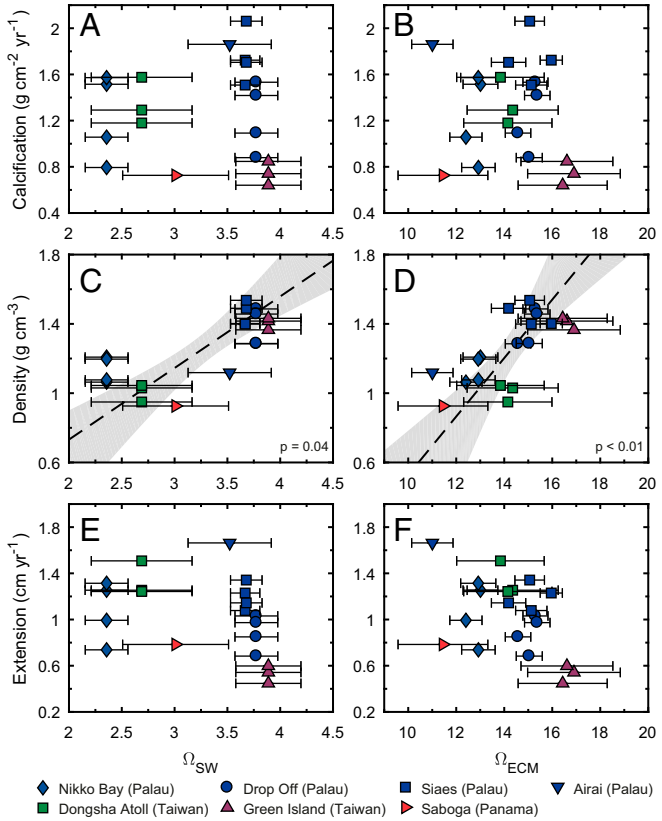

Fig. 1. Coral skeletal parameters measured in representative *Porites* cores from four reefs across the Pacific. Coral calcification rates do not correlate with either Ω_{sw} or Ω_{ECM} (*A* and *B*). Instead, skeletal density exhibits a significant positive correlation with both Ω_{sw} and Ω_{ECM} (*C* and *D*), but extension does not (*E* and *F*; $P = 0.14$ and $P = 0.09$, respectively). Individual points represent annual averages of skeletal growth. Error bars denote 1 SD of Ω propagated from seasonal variability in seawater physicochemical parameters (for Ω_{sw} and Ω_{ECM}) and in boron isotope compositions of coral skeletons (for Ω_{ECM}).

These observations, although counterintuitive, are consistent with the two-step model of coral calcification, in which coral skeleton is accreted in two distinct phases (31): vertical upward growth (i.e., extension) creating new skeletal elements and lateral thickening of existing elements in contact with living tissue. These two components of coral growth are fundamentally different processes. Skeletal extension is driven by the accretion of successive, elongated early mineralization zones (EMZs; also referred to as centers of calcification and the immediately associated fibers) in a continuous or semicontinuous column parallel to the upward growth axis of the skeleton (17, 32, 33). Conversely, skeletal thickening occurs via growth of bundles of mature, *c* axis-aligned aragonite fibers at an angle that is perpendicular or semiperpendicular to the EMZ and upward growth axis of the coral. This thickening affects the bulk density of the skeleton, because the more the fiber bundles thicken or lengthen, the lower the skeletal porosity (Fig. S2) (17, 33, 34). Our data reveal the strong sensitivity of skeletal density to ECM carbonate chemistry and ocean acidification (Fig. 1). Conversely, skeletal extension seems less sensitive or insensitive to ECM carbonate chemistry. One explanation for this finding is that the EMZs, which contain a relatively high concentration of organic material (34–36), are under stronger biological control (37–39) and are thus shielded from changes in calcifying fluid pH and external seawater pH. Conversely, weaker biological control of fiber bundle growth would render skeletal density more exposed to physicochemical influences and thus, more sensitive to changes in both calcifying fluid pH and ocean acidification.

Results of experimental studies support this hypothesis. Laboratory experiments showed no decline in the extension rate of *Stylophora pistillata* over a year of growth in low-Ω_{sw} seawater (1.1–3.2) (7). Similarly, most field studies, except one (14), have found no significant effect of ocean acidification on coral skeletal extension over pH ranges expected in the 21st century (9–11, 29). Instead, the extension is believed to be controlled by other environmental factors, such as irradiance, temperature, and nutrient environment (40). For example, studies show that coral extension rates decline exponentially with water depth over a range of ~40 m after light attenuation (41–43) but increase with mean annual sea surface temperature (SST) until an optimum thermal threshold (44, 45). In addition, sediment influx and nutrient loading have also been suggested to influence extension rates in a nonlinear fashion, with minor increases in nutrient availability promoting growth and more severe nutrient loading leading to abrupt declines (46). We, however, observe none of these correlations in our coral cores, presumably due to the small depth and temperature ranges that they cover (i.e., 1–6 m and 26.4 °C to 30.3 °C) (Table S1).

Our observation that skeletal density but not extension is affected by seawater chemistry may explain the large variability in the response of coral calcification to ocean acidification, as calcification is calculated as the product of linear extension and mean skeletal density. Our findings are consistent with previous suggestions that

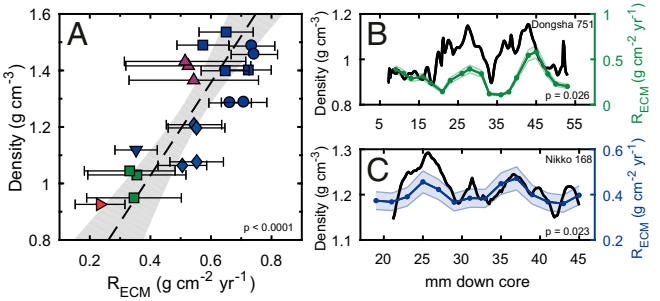

Fig. 2. Correlation between coral skeletal density and expected aragonite precipitation rate in the coral ECM (R_{ECM}) on both the annual (*A*) and seasonal (*B* and *C*) scales. Data in *A* represent the same cores as in Fig. 1. Error bars (*A*) and shaded areas (*B* and *C*) denote 1 SD in R_{ECM} as propagated from uncertainties in seawater parameters and in boron isotope measurements. Seasonal density profiles were retrieved parallel to the sampling track for boron isotope measurements.

the accretion of EMZ during coral calcification is under stronger biological control (17, 34–36), presumably through the organic matrix (47–49), and also with previous reports of the sensitivity of skeletal porosity to ocean acidification (7, 29). Furthermore, because density is a critical component of the coral growth process, our results support laboratory and field-based studies that report negative impacts of ocean acidification on coral calcification and consequently, the health of coral reef ecosystems (12).

A Numerical Model of *Porites* Skeletal Growth. Within the two-step model of coral calcification, coral skeletal density is strongly controlled by the rate of skeletal thickening, which is expected to vary as a function of Ω_{ECM}:

$$R_{ECM} = k(\Omega_{ECM} - 1)^n, \quad [1]$$

where R_{ECM} is the expected aragonite precipitation rate in the ECM, and k and n are the rate constant and reaction order for aragonite precipitation, respectively (5). This is confirmed by the significant correlation between skeletal density and expected aragonite precipitation rate in our cores on both annual and seasonal scales, providing a mechanistic link between skeletal density and seawater chemistry subsequent to its modulation in the ECM (Fig. 2).

To quantitatively evaluate the sensitivity of skeletal density to ocean acidification, we construct a numerical model of *Porites* skeletal growth that builds on previous modeling studies (e.g., ref. 50) (Fig. 3*A* and *SI Text*). In this model, the coral calyx is approximated as a ring in which coral growth proceeds in two consecutive steps: vertical construction of new skeletal framework representing daily extension of EMZs (E) followed by lateral aragonite precipitation around the interior of the ring representing thickening. Thickening of the skeletal elements, which we prescribe an initial ring wall thickness of w_o, occurs throughout the tissue layer—most prominently at the polyp surface and diminishing with depth (31, 51):

$$R(z) = R_{ECM} \times e^{-\frac{\lambda \times z}{T_d}}, \quad [2]$$

where $R(z)$ is the aragonite precipitation rate at depth z, λ is the decay constant, and T_d is the thickness of the coral tissue layer. In our model, T_d is stretched daily coincident with skeletal extension and reset at monthly intervals to simulate dissepiment formation and subsequent vertical migration of polyps (52, 53). The final density of coral skeleton when exiting the tissue layer is then calculated as the fraction of filled calyx:

$$\rho_{coral} = \rho_{arag}\left(1 - \frac{r_f^2}{r_o^2}\right), \quad [3]$$

where ρ_{arag} is the density of aragonite and r_f and r_o represent the inner and outer radii of the calyx, respectively (Fig. 3*A*).

Within this model framework, five key factors control the density of coral skeleton: initial calyx size (r_o), thickness of the new skeletal framework (w_o), aragonite precipitation rate in the ECM (R_{ECM}), decline of thickening rate from the surface to the depth of the tissue layer (λ), and the time that a skeletal element spends within the tissue layer ($t = T_d/E$). R_{ECM} is calculated based on seawater physicochemical parameters, pH of the ECM, and the DIC elevation factor (i.e., α) in the ECM and assumes that the sensitivity of coral aragonite formation to the ECM carbonate chemistry is the same as that determined in abiotic precipitation experiments (*Methods* and Eq. **1**) (6, 32, 37). Most of these model parameters (e.g., r_o, T_d, E) can be accurately determined via computed tomography (CT) imaging and inspection of each coral core. However, there are limited experimental constraints on the other parameters, including w_o, λ, and α. We assume that these three parameters are the same for all *Porites* corals and optimize their values to reproduce the measured skeletal density of our cores via a Bayesian statistical method (*SI Text*). Our estimated α value ($2.05^{+0.39}_{-0.38}$, 2σ) is similar to the experimentally estimated DIC elevation factor for *Porites* [e.g., 1.4 ± 0.1 (26) or 2.6 ± 0.6 (27)]. However, the estimated value of w_o (59^{+23}_{-24} μm), which translates to 37–49% of the total skeleton, is approximately twice that estimated from visual observation of the EMZs in SEM images and petrographic thin sections (Fig. S2). This difference likely reflects the stacking of different skeletal elements in the simplified ring geometry assumed in our model and the normalization of the whole sensitivity spectrum of different skeletal components to ECM

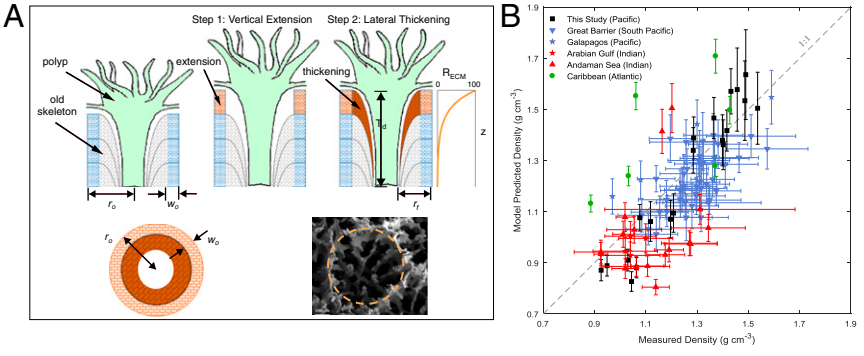

Fig. 3. Schematic representation of our *Porites* skeletal growth model (*A*) and comparison between model-predicted skeletal density and measured density (*B*). Also shown in *A* are a cross-section view of our model polyp geometry and a representative SEM image of a *Porites* calyx (orange dashed line). *Porites* cores in *B* were collected from reefs in the Pacific, Atlantic, and Indian Oceans reported in previous studies (9, 30, 54–57). Data points from this study, the Caribbean, and the Andaman Sea represent densities of individual cores; data points from the Galapagos, the Great Barrier Reef, and the Andaman Sea represent site average densities for which error bars denote 2σ uncertainties. Vertical error bars represent uncertainties in model prediction propagated from uncertainties in model parameters α, λ, and w_o as well as measurements of in situ seawater conditions where available. Where seawater conditions were not reported, outputs from the CESM-BGC historical run were adopted.

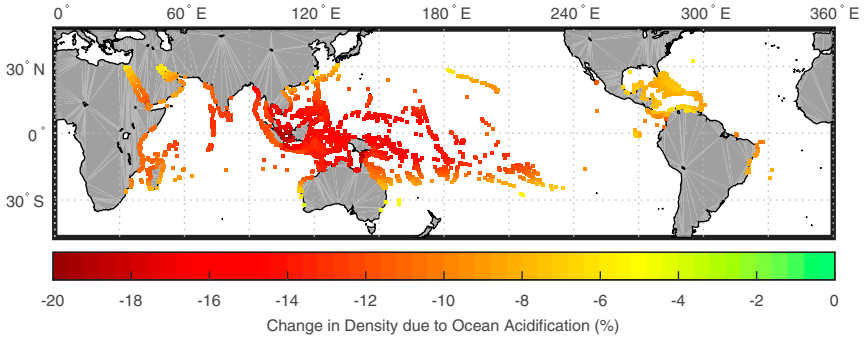

Fig. 4. Model-predicted decline in *Porites* skeletal density over the 21st century due to ocean acidification. Our model predicts an average 12.4 ± 5.8% (2σ) decline in density across global reef sites, with the largest decline in the western tropical Pacific coral triangle region (an average of ~14% and a maximum of 20.3%) and the least in the Caribbean (~6%). Simulations were conducted based on outputs from the CESM-BGC RCP 8.5 run for the years 2006–2015 and 2090–2099 (*Methods*). Skeletal extension, initial radius, and tissue thickness were held constant in these simulations. Error represents only that propagated from estimation of model parameters.

carbonate chemistry into two simplified groups in our model: not sensitive (i.e., "initial framework") and highly sensitive (i.e., "thickening"). The exact sensitivity prescribed to the highly sensitive group (Eq. **1**) also affects the estimated w_o value. Our analysis also provides quantitative estimates of λ ($12.8^{+11.9}_{-6.2}$), suggesting a 50% decrease in skeletal thickening rate at a depth of 4–12% into the tissue layer. With these estimated parameters, our model can quantitatively predict *Porites* skeletal densities under different seawater conditions.

To evaluate the performance of our model, we use it to predict the skeletal densities of *Porites* corals at five tropical reefs and compare our model-predicted densities with the experimentally measured densities reported in previous studies (Fig. 3*B* and Fig. S6) (9, 30, 54–57). These studies were selected, because they report not only coral skeletal density but also, extension and at least one of the following factors needed for our model prediction: r_o, T_d, or in situ seawater carbonate chemistry. This minimizes the uncertainty in our model prediction propagated from estimations of unmeasured parameters (*Methods*). Corals in these studies consist of six different *Porites* species and represent a wide range of reef environments across the Atlantic, Pacific, and Indian Ocean basins (21.7° S to 22.6° N), with large variations in annual SST (22.3 °C to 29.5 °C), pH (7.20–8.24), DIC (1,780–3,170 μmol kg^{-1}), and coral skeletal density (0.9–1.6 g cm^{-3}).

Our model predictions quantitatively reproduce the experimentally measured coral densities and explain a large amount of the variance in the measured densities (Fig. 3*B*) [root-mean-square error (RMSE) = 0.15, r^2 = 0.494, $P < 0.0001$]. The exact agreements between modeled and measured densities vary between studies and are related to the uncertainties in the unmeasured parameters in each study. Among these parameters, r_o has the strongest effect on the model-predicted density, producing about −1% change in density for every 1% change in r_o. The model is less sensitive to R_{ECM} and T_d, yielding about 0.54 and 0.28% changes in density for every 1% change in each parameter, respectively (Fig. S5). Three parameters, w_o, λ, and α, were held constant in the model simulations for all studies. However, only two of the six species examined in these studies (i.e., *Porites lobata*, *Porites lutea*) were included in our estimation of these three parameters, which could introduce additional uncertainties in our model predictions. Accordingly, we observe better agreements between model-predicted density and measured density for studies in which skeletal and physiochemical parameters are well-constrained and that are dominated by the same species as this study (e.g., the Arabian Gulf and Great Barrier Reef studies) (Fig. S6). In contrast, locations with poor constraints on r_o, T_d, and R_{ECM} (e.g., the Andaman Sea and the Caribbean region) yield less satisfactory agreements.

Other than the parameters discussed above, the rate of skeletal extension that was measured in all of these studies also affects coral skeletal density, as it influences the amount of time that each skeletal element spends inside the coral tissue layer subject to thickening ($t = T_d/E$). Although we do not observe significant correlations between skeletal density and extension rate in our *Porites* cores on either annual or seasonal scales, as were observed in some previous studies (55, 57), two of the six studies included in our model–data comparison show apparent correlations between annual density and extension (Fig. S7). When examined as a whole, skeletal data from most of these studies also show an apparent correlation between these two parameters across the large range of extension (~0.2–2.3 cm y^{-1}) (Fig. S7), yielding a sensitivity of −0.20% change in density for every 1% change in extension. This observed correlation is consistent with our model-predicted sensitivity of skeletal density to extension [i.e., −0.30% change in density for 1% change in extension (Fig. S5)] and contributes to the agreement between our model-predicted density and experimentally measured density.

Projecting the Impact of Ocean Acidification on *Porites* Skeletal Density. Our model takes into account the different factors that can influence *Porites* coral skeletal growth (e.g., seawater conditions, extension, polyp geometry) and enables us to isolate and evaluate the influence of each factor. Here, we use it to evaluate the response of *Porites* coral skeletal density to ocean acidification by forcing our model with outputs from the Community Earth System Model Biogeochemical (CESM-BGC) run in the RCP 8.5 projection (i.e., the business as usual emission scenario). Among global reef sites, the CESM-BGC run predicts a 0.25 to 0.35 units decrease in seawater pH, a −50 to 250 μmol/kg change in DIC, and a 1.7 °C to 3 °C increase in SSTs by the end of the 21st century. These translate to a 0.85–1.95 decrease in seawater aragonite saturation states. There remain large uncertainties in how rising SSTs will affect coral calcification via its effects on zooxanthellae photosynthesis and coral bleaching (58–60). Thus, we focus solely on the impact of ocean acidification on coral skeletal density and do not include the effects of temperature on the reaction kinetics of aragonite precipitation in the following model simulations (*SI Text*). For the similar reasons, all model parameters (i.e., r_o, T_d, E, λ, w_o, and α) were held constant in these simulations.

Our simulations predict an average 12.4 ± 5.8% (2σ) decline in *Porites* skeletal density across global reef sites by the end of the 21st century due to ocean acidification alone (Fig. 4). This decline results from the interplay between changes in seawater pH and DIC, with decreases in pH leading to an average decline in density of 16.8 ± 4.7% mitigated by increasing DIC, which drives a 6.4 ± 3.7% increase in density. Our model predicted that density declines vary among different reefs, with equatorial reefs generally more impacted than higher-latitude reefs. For example, our model predicts the largest decreases in skeletal density (11.4–20.3%) in the coral triangle region driven by the largest pH decreases projected for this region (up to 0.35 units). In contrast, reefs in the Caribbean and the Arabian Gulf are predicted to experience no significant decline in coral skeletal density. In these regions, the effect of relatively small projected pH decrease (~0.29 units on average) is balanced by the largest

increases in DIC (~175 μmol/kg on average). The model-predicted density changes also vary across reef systems. For example, up to 13% density decline is predicted in the northern Great Barrier Reef, while no significant change is predicted in the southern edges.

Our results suggest that ocean acidification alone would lead to declines in *Porites* coral skeletal density over the 21st century. Such declines in skeletal density could increase the susceptibility of coral reef ecosystems to bioerosion, dissolution, and storm damage (61–63). It is important to note that, in addition to ocean acidification, coral reefs today face many other environmental stressors, including changes in temperature, nutrient concentration, and sea level (40). Our model enables us to isolate the impact of ocean acidification on coral skeletal growth. With accurate incorporation of the impacts of these other stressors, future models of this kind will be able to quantitatively project the fate of reef ecosystems under 21st century climate change.

Methods

Coral Samples and Reef Sites. Nine 3-cm-diameter *Porites* cores were collected from reefs in Palau (six cores from four different sites), Donghsa Atoll (one core), Green Island (one core), and Isla Saboga (one core). For Palau sites, seawater salinity and carbonate chemistry parameters were acquired from 4 y of discrete sampling at each site (11), and seawater temperatures were derived from the National Oceanic and Atmospheric Administration Optimum Interpolation Sea Surface Temperature (oiSST) dataset after correcting for any mean and variance bias during overlapping periods of in situ logger temperatures (64). At other reef sites, seawater salinity and carbonate chemistry parameters were either determined based on discrete samples of seawater collected during coring and on subsequent visits to the respective reefs or compiled from reported values in the literature (Table S1). Seawater temperatures for these sites were derived from the oiSST dataset and were assumed to be representative of in situ reef conditions, since no temperature loggers were deployed and satellite SST agreed reasonably with literature values. Total alkalinity and DIC of all seawater samples were measured on a Versatile Instrument for Determination of Total inorganic Carbon at Woods Hole Oceanographic Institution with the open cell potentiometric and coulometric titration method. Seawater pH and aragonite saturation states were then calculated using the CO2SYS program (65).

Determination of Coral Skeletal Growth Parameters. Coral cores were imaged with a Siemens Volume Zoom Spiral Computerized Tomography scanner to determine skeletal density and to identify annual density bands. Annual extension rates, skeletal density, and calcification rates were then determined based on these CT images along polyp growth axes (66) (Table S1). Specifically, annual extension rate (E_A) was calculated as the average length of corallite traces between consecutive low-density band surfaces, and annual density ($\overline{\rho}_A$) was measured along each continuous corallite trace and averaged across corallites to avoid density anomalies from bioerosion or secondary crystallization. Annual calcification rates (C_A) were taken as the product of annual extension rate and density $C_A = E_A \times \overline{\rho}_A$. Average corallite areas were also calculated by identifying local density minima in each image, which correspond to porous calix centers, and assigning each nearby voxel to the closest density minimum. Because our skeletal growth model approximates corallite geometry as a ring, radii of each corallite were calculated assuming a circular geometry.

Boron Isotope Measurements. Each core was sampled at ~1-mm intervals for boron isotope measurements over at least one annual density band couplet, resulting in 6–10 measurements in each annual band (Table S1). The isotope measurements were conducted at the Thermo Scientific Neptune multi-collector ICP-MS either at Academia Sinica (Taiwan) or at National Oceanography Centre Southampton (67). The pH of the ECM was then estimated based on the measured δ^{11}B values:

$$\mathrm{pH_{ECM}} = \mathrm{pK_B^*} - \log\left(-\frac{\delta^{11}\mathrm{B}_{SW} - \delta^{11}\mathrm{B}_{coral}}{\delta^{11}\mathrm{B}_{SW} - \alpha_B\delta^{11}\mathrm{B}_{coral} - ([\alpha_B - 1] \times 1{,}000)}\right),$$

where $\mathrm{pK_B^*}$ is the equilibrium constant for the dissociation reaction of boric acid to borate estimated at respective seawater temperature and salinity (68), and the δ^{11}B of seawater was taken to be 39.61‰ (69). The boron isotope fractionation factor, α_B, is assumed to be 1.0272 (70).

Estimation of Aragonite Precipitation Rate in ECM. Aragonite precipitation rate in the ECM (R_{ECM}) was calculated based on ECM aragonite saturation state (Ω_{ECM}) (Eq. **1**), using the rate constants and reaction orders determined in laboratory carbonate precipitation experiments by ref. 5 and fit by ref. 22:

$$k = -0.0177T^2 + 1.47T + 14.9, n = 0.0628T + 0.0985.$$

Aragonite saturation state in the ECM was estimated as

$$\Omega_{\mathrm{ECM}} = \frac{[\mathrm{Ca^{2+}}]_{\mathrm{ECM}} \times [\mathrm{CO_3^{2-}}]_{\mathrm{ECM}}}{K_{sp}},$$

where K_{sp} is the solubility product of aragonite in seawater at the corresponding temperature and salinity (71), and $[\mathrm{CO_3^{2-}}]_{\mathrm{ECM}}$ and $[\mathrm{Ca^{2+}}]_{\mathrm{ECM}}$ are the calcium and carbonate ion concentrations in the ECM, respectively. $[\mathrm{Ca^{2+}}]_{\mathrm{ECM}}$ was assumed to be the same as seawater that was estimated from seawater salinity (72). $[\mathrm{CO_3^{2-}}]_{\mathrm{ECM}}$ was calculated based on the $\mathrm{pH_{ECM}}$ derived from boron isotope measurements, seawater temperature, salinity, and DIC with a DIC elevation factor of $\alpha = 2$, using CO2SYS program (65) with the equilibrium constants determined in ref. 71 and refit by ref. 73.

Estimation of Model Parameters with Bayesian Methods. Three parameters in our coral skeletal growth model were estimated with a Bayesian inference method (*SI Text*). These are the thickness of each new skeletal framework (w_o), the decline of thickening rate with depth within the tissue layer (λ), and the DIC elevation factor in the ECM (α). Prior distributions for each parameter were constructed based on constraints from existing studies and were combined to form a joint prior distribution. The likelihood of each combination of parameters was then evaluated by comparing measured densities in our cores with the associated model predictions. The prior distribution was updated using the likelihood function via Bayes' Theorem to form a posterior distribution, from which the most likely values for each parameter were acquired.

Comparison of Model Prediction with Existing Studies. *Porites* corals from five reefs reported in six previous studies were used to evaluate the accuracy of our skeletal growth model in predicting coral skeletal density. These corals were collected from reefs in the Galapagos, the Andaman Sea, the Great Barrier Reef, the Caribbean, and the Arabian Gulf (9, 30, 54–56, 74). Other than the three parameters estimated above with Bayesian methods, other parameters required for our model prediction include E, r_o, T_d, seawater temperature, salinity, and carbonate chemistry (from which R_{ECM} is calculated). Among these, only E was reported in all of the studies. When not reported, r_o and T_d values were estimated either from studies conducted at nearby reef sites or from taxonomic averages for each species (details are in *SI Text*). In situ measurements of seawater carbonate chemistry, SST, and salinity, whenever available, were used to calculate R_{ECM}; when not available, pH, DIC, salinity, and temperature outputs from the CESM-BGC run were averaged over the time period that skeletal growth parameters were measured and used to estimate R_{ECM}. As none of these studies determined carbonate chemistry of the coral ECM, we estimated the coral $\mathrm{pH_{ECM}}$ based on the $\mathrm{pH_{ECM}} \sim \mathrm{pHsw}$ correlation observed in laboratory *Porites* manipulation experiments (23), which cover a $\mathrm{pH_{sw}}$ range similar to these studies (i.e., 7.19–8.09 vs. 7.23–8.15).

Projection of Future Skeletal Density Changes for Global Reefs. Changes in skeletal density on different reefs over the 21st century were predicted based on output from the CESM-BGC RCP 8.5 run. Monthly projections of DIC, pH, T, and S from the first 10 y (2006–2015) and the last 10 y (2090–2099) of the run were extracted from the 1° × 1° model and averaged to represent the current and end of century seawater conditions at different reef sites around the globe. Reef site locations are provided by the ReefBase database of reef sites (75). Skeletal growth parameters, E (annual extension rate), T_d (tissue thickness), and r_o (polyp radii), were prescribed at 1.0 cm y^{-1}, 0.56 cm, and 0.063 cm, respectively, (the average values observed in our cores) and were held constant for predictions over the 21st century. The effect of temperature on the kinetics of aragonite precipitation was not considered in the model simulation. A detailed analysis of the effects of the projected 21st century warming on model predictions is presented in *SI Text*.

ACKNOWLEDGMENTS. We thank Pat Lohmann and Kathryn Pietro (Woods Hole Oceanographic Institution), Jay Andrew (Palau International Coral Reef Center), and Edgardo Ochoa (Smithsonian Tropical Research Institute) for assistance with coral core collection. This research was supported by US National Science Foundation Award OCE-1220529, the Robertson Foundation, Woods Hole Oceanographic Institution through the Ocean Life Institute, Investment in Science Fund and Early Career Award, Taiwan MOST Grant 104-2628-M-001-007-MY3, and the Leverhulme Trust in UK.

1. Doney SC, Fabry VJ, Feely RA, Kleypas JA (2009) Ocean acidification: The other CO2 problem. *Annu Rev Mar Sci* 1:169–192.
2. Kleypas J (1999) Geochemical consequences of increased atmospheric carbon dioxide on coral reefs. *Science* 284:118–120.
3. Hoegh-Guldberg O, et al. (2007) Coral reefs under rapid climate change and ocean acidification. *Science* 318:1737–1742.
4. Meissner KJ, Lippmann T, Sen Gupta A (2012) Large-scale stress factors affecting coral reefs: Open ocean sea surface temperature and surface seawater aragonite saturation over the next 400 years. *Coral Reefs* 31:309–319.
5. Burton EA, Walter LM (1987) Relative precipitation rates of aragonite and Mg calcite from seawater: Temperature or carbonate ion control? *Geology* 15:111–114.
6. Comeau S, Edmunds PJ, Spindel NB, Carpenter RC (2014) Fast coral reef calcifiers are more sensitive to ocean acidification in short-term laboratory incubations. *Limnol Oceanogr* 59:1081–1091.
7. Tambutté E, et al. (2015) Morphological plasticity of the coral skeleton under CO2-driven seawater acidification. *Nat Commun* 6:7368.
8. Langdon C, et al. (2000) Effect of calcium carbonate saturation state on the rate of calcification of an experimental coral reef. *Global Biogeochem Cycles* 14:639–654.
9. Crook ED, Cohen AL, Rebolledo-Vieyra M, Hernandez L, Paytan A (2013) Reduced calcification and lack of acclimatization by coral colonies growing in areas of persistent natural acidification. *Proc Natl Acad Sci USA* 110:11044–11049.
10. Fabricius KE, et al. (2011) Losers and winners in coral reefs acclimatized to elevated carbon dioxide concentrations. *Nat Clim Chang* 1:165–169.
11. Barkley HC, et al. (2015) Changes in coral reef communities across a natural gradient in seawater pH. *Sci Adv* 1:e1500328.
12. Chan NCS, Connolly SR (2013) Sensitivity of coral calcification to ocean acidification: A meta-analysis. *Glob Chang Biol* 19:282–290.
13. Pandolfi JM, Connolly SR, Marshall DJ, Cohen AL (2011) Projecting coral reef futures under global warming and ocean acidification. *Science* 333:418–422.
14. Enochs IC, et al. (2015) Shift from coral to macroalgae dominance on a volcanically acidified reef. *Nat Clim Change* 5:1–9.
15. Lough JM (2008) Coral calcification from skeletal records revisited. *Mar Ecol Prog Ser* 373:257–264.
16. Allemand D, Tambutté É, Zoccola D, Tambutté S (2011) Coral calcification, cells to reefs. *Coral Reefs: An Ecosystem in Transition*, eds Dubinsky Z, Stambler N (Springer, Dordrecht, The Netherlands), pp 119–150.
17. Cohen AL, McConnaughey TA (2003) Geochemical perspectives on coral mineralization. *Rev Mineral Geochem* 54:151–187.
18. Constantz BR (1986) Coral skeleton construction: A physiochemically dominated process. *Palaios* 1:152–157.
19. Gattuso J-P, Allemand D, Frankignoulle M (1999) Photosynthesis and calcification at cellular, organismal and community levels in coral reefs: A review on interactions and control by carbonate chemistry. *Am Zool* 39:160–183.
20. Tambutté S, et al. (2007) Characterization and role of carbonic anhydrase in the calcification process of the azooxanthellate coral Tubastrea aurea. *Mar Biol* 151:71–83.
21. Tambutté S, et al. (2011) Coral biomineralization: From the gene to the environment. *J Exp Mar Biol Ecol* 408:58–78.
22. McCulloch M, Falter J, Trotter J, Montagna P (2012) Coral resilience to ocean acidification and global warming through pH up-regulation. *Nat Clim Change* 2:623–627.
23. Trotter J, et al. (2011) Quantifying the pH "vital effect" in the temperate zooxanthellate coral Cladocora caespitosa: Validation of the boron seawater pH proxy. *Earth Planet Sci Lett* 303:163–173.
24. Hönisch B, et al. (2004) Assessing scleractinian corals as recorders for paleo-pH: Empirical calibration and vital effects. *Geochim Cosmochim Acta* 68:3675–3685.
25. Venn A, Tambutté E, Holcomb M, Allemand D, Tambutté S (2011) Live tissue imaging shows reef corals elevate pH under their calcifying tissue relative to seawater. *PLoS One* 6:e20013.
26. Allison N, Cohen I, Finch AA, Erez J, Tudhope AW; Edinburgh Ion Microprobe Facility (2014) Corals concentrate dissolved inorganic carbon to facilitate calcification. *Nat Commun* 5:5741.
27. Mcculloch MT, Olivo JPD, Falter J, Holcomb M, Trotter JA (2017) Coral calcification in a changing world and the interactive dynamics of pH and DIC upregulation. *Nat Commun* 8:15686.
28. Cai WJ, et al. (2016) Microelectrode characterization of coral daytime interior pH and carbonate chemistry. *Nat Commun* 7:11144.
29. Fantazzini P, et al. (2015) Gains and losses of coral skeletal porosity changes with ocean acidification acclimation. *Nat Commun* 6:7785.
30. Manzello DP, et al. (2014) Galapagos coral reef persistence after ENSO warming across an acidification gradient. *Geophys Res Lett* 41:9001–9008.
31. Barnes DJ, Lough JM (1993) On the nature and causes of density banding in massive coral skeletons. *J Exp Mar Biol Ecol* 167:91–108.
32. Wells JW (1956) Scleractinia. *Treatise on Invertebrate Paleontology F. Coelenterata*, ed Moore RC (Geology Society of American and Univ of Kansas Press, Lawrence, KS), pp 328–440.
33. Northdruft LD, Webb GE (2007) Microstructure of common reef-building coral genera Acropora, Pocillopora, Goniastrea and Porites: Constraints on spatial resolution in geochemical sampling. *Facies* 53:1–26.
34. Stolarski J (2003) Three-dimensional micro- and nanostructural characteristics of the scleractinian coral skeleton: A biocalcification proxy. *Acta Palaeontol Pol* 48:497–530.
35. Cuif JP, Dauphin YY, Doucet J, Salome M, Susini J (2003) XANES mapping of organic sulfate in three scleractinian coral skeletons. *Geochim Cosmochim Acta* 67:75–83.
36. Shirai K, et al. (2012) Visualization of sub-daily skeletal growth patterns in massive Porites corals grown in Sr-enriched seawater. *J Struct Biol* 180:47–56.
37. Clode PL, Marshall AT (2002) Low temperature FESEM of the calcifying interface of a scleractinian coral. *Tissue Cell* 34:187–198.
38. Clode PL, Marshall AT (2003) Calcium associated with a fibrillar organic matrix in the scleractinian coral Galaxea fascicularis. *Protoplasma* 220:153–161.
39. van de Locht R, et al. (2013) Microstructural evolution and nanoscale crystallography in scleractinian coral spherulites. *J Struct Biol* 183:57–65.
40. Lough JM, Cooper TF (2011) New insights from coral growth band studies in an era of rapid environmental change. *Earth Sci Rev* 108:170–184.
41. Huston M (1985) Variation in coral growth rates with depth at Discovery Bay, Jamaica. *Coral Reefs* 4:19–25.
42. Dustan P (1975) Growth and form in the reef-building coral Montastrea annularis. *Mar Biol* 33:101–107.
43. Al-Rousan S (2012) Skeletal extension rate of the reef building coral Porites species from Aqaba and their environmental variables. *Nat Sci* 4:731–739.
44. Cantin NE, Cohen AL, Karnauskas KB, Tarrant AM, McCorkle DC (2010) Ocean warming slows coral growth in the central Red Sea. *Science* 329:322–325.
45. Cooper TF, De'ath G, Fabricius KE, Lough JM (2008) Declining coral calcification in massive Porites in two nearshore regions of the northern Great Barrier Reef. *Glob Chang Biol* 14:529–538.
46. Tomascik T, Sander F (1985) Effects of eutrophication on reef-building corals. *Mar Biol* 87:143–155.
47. Euw SVon, et al. (2017) Biological control of aragonite formation in stony corals. *Science* 356:933–938.
48. Allemand D, TambuttE E, Girard JP, Jaubert J (1998) Organic matrix synthesis in the scleractinian coral *Stylophora pistillata*: Role in biomineralization and potential target of the organotin tributyltin. *J Exp Biol* 201:2001–2009.
49. Watanabe T, Fukuda I, China K, Isa Y (2003) Molecular analyses of protein components of the organic matrix in the exoskeleton of two scleractinian coral species. *Comp Biochem Physiol B Biochem Mol Biol* 136:767–774.
50. Taylor RB, Barnes DJ, Lough JM (1993) Simple-models of density band formation in massive corals. *J Exp Mar Biol Ecol* 167:109–125.
51. Gagan MK, Dunbar GB, Suzuki A (2012) The effect of skeletal mass accumulation in Porites on coral Sr/Ca and $\delta^{18}O$ paleothermometry. *Paleoceanography* 27:PA1203.
52. Sorauf J (1970) Microstructure and formation of dissepiments in the skeleton of the recent scleractinia (hexacorals). *Biomineralization* 2:1–22.
53. Buddemeier RW, Maragos JE, Knutson DW (1974) Radiographic studies of reef coral exoskeletons: Rates and patterns of coral growth. *J Exp Mar Biol Ecol* 14:179–199.
54. Tanzil JTI, et al. (2013) Regional decline in growth rates of massive Porites corals in Southeast Asia. *Glob Chang Biol* 19:3011–3023.
55. Lough JM, Barnes DJ (2000) Environmental controls on growth of the massive coral Porites. *J Exp Mar Biol Ecol* 245:225–243.
56. Poulsen A, Burns K, Lough J, Brinkman D, Delean S (2006) Trace analysis of hydrocarbons in coral cores from Saudi Arabia. *Org Geochem* 37:1913–1930.
57. Decarlo TM, Cohen AL (2017) Dissepiments, density bands, and signatures of thermal stress in Porites skeletons. *Coral Reefs* 38:749–761.
58. Warner ME, Fitt WK, Schmidt GW (1996) The effects of elevated temperature on the photosynthetic efficiency of zooxanthellae in hospite from four different species of reef coral: A novel approach. *Plant Cell Environ* 19:291–299.
59. Coles SL, Jokiel PL (1977) Effects of temperature on photosynthesis and respiration in hermatypic corals. *Mar Biol* 43:209–216.
60. Van Hooidonk R, et al. (2016) Local-scale projections of coral reef futures and implications of the Paris Agreement. *Sci Rep* 6:39666.
61. Sammarco P, Risk M (1990) Large-scale patterns in internal bioerosion of Porites: Cross continental shelf trends on the Great Barrier Reef. *Mar Ecol Prog Ser* 59:145–156.
62. van Woesik R, van Woesik K, van Woesik L, van Woesik S (2013) Effects of ocean acidification on the dissolution rates of reef-coral skeletons. *PeerJ* 1:e208.
63. Madin JS, Hughes TP, Connolly SR (2012) Calcification, storm damage and population resilience of tabular corals under climate change. *PLoS One* 7:e46637.
64. Reynolds RW, et al. (2007) Daily high-resolution-blended analyses for sea surface temperature. *J Clim* 20:5473–5496.
65. Pierrot D, Lewis E, Wallace DWR (2006) MS Excel Program Developed for CO2 System Calculations (Oak Ridge National Laboratory, Oak Ridge, TN). ORNL/CDIAC-105a.
66. Decarlo TM (2016) coralCT: Software Tool to Analyze Computerized Tomography (CT) Scans of Coral Skeletal Cores for Calcification and Bioerosion Rates. Version 1.1. Available at https://zenodo.org/record/57855. Accessed January 17, 2016.
67. Foster GL, Rae J, Elliot T (2008) Boron isotope measurements of marine carbonate using MC-ICPMS. *Geochim Cosmochim Acta* 72:279.
68. Dickson AG (1990) Thermodynamics of the dissociation of boric acid in synthetic seawater from 273.15 to 318.15 K. *Deep Sea Res Part A* 37:755–766.
69. Foster GL, Pogge Von Strandmann PAE, Rae JWB (2010) Boron and magnesium isotopic composition of seawater. *Geochem Geophys Geosyst* 11:Q08015.
70. Klochko K, Kaufman AJ, Yao W, Byrne RH, Tossell JA (2006) Experimental measurement of boron isotope fractionation in seawater. *Earth Planet Sci Lett* 248:261–270.
71. Mehrbach C, Culberson CH, Hawley JE, Pytkowicz RM (1973) Measurement of the apparent dissociation constants of carbonic acid in seawater at atmospheric pressure. *Limnol Oceanogr* 18:897–907.
72. Krumgalz BS (1982) Calcium distribution in the world ocean waters. *Oceanol Acta* 5: 121–128.
73. Dickson AG, Millero FJ (1987) A comparison of the equilibrium constants for the dissociation of carbonic acid in seawater media. *Deep Sea Res Part A* 34:1733–1743.
74. Tanzil JTI, Brown BE, Tudhope AW, Dunne RP (2009) Decline in skeletal growth of the coral Porites lutea from the Andaman Sea, South Thailand between 1984 and 2005. *Coral Reefs* 28:519–528.
75. McManus JM, Ablan MC (1996) ReefBase: A global database on coral reefs and their resources. Available at www.reefbase.org/global_database/. Accessed August 18, 2016.